ELSEVIER

Biochimica et Biophysica Acta 1509 (2000) 275–291

BIOCHIMICA ET BIOPHYSICA ACTA

BBA

www.elsevier.com/locate/bba

Contributions of charged residues in a cytoplasmic linking region to Na channel gating

James R. Miller, Manoj K. Patel, James E. John, J. Paul Mounsey, J. Randall Moorman *

Department of Internal Medicine (Cardiovascular Division) and Department of Molecular Physiology and Biological Physics, University of Virginia Health Sciences Center, Box 6012, MR4 Building, 300 Park Place, Charlottesville, VA 22908, USA

Received 11 November 1999; received in revised form 25 July 2000; accepted 25 July 2000

Abstract

Na channels inactivate quickly after opening, and the very highly positively charged cytoplasmic linking region between homologous domains III and IV of the channel molecule acts as the inactivation gate. To test the hypothesis that the charged residues in the domain III to domain IV linker have a role in channel function, we measured currents through wild-type and two mutant skeletal muscle Na channels expressed in *Xenopus* oocytes, each lacking two or three charged residues in the inactivation gate. Microscopic current measures showed that removing charges hastened activation and inactivation. Macroscopic current measures showed that removing charges altered the voltage dependence of inactivation, suggesting less coupling of the inactivation and activation processes. Reduced intracellular ionic strength shifted the midpoint of equilibrium activation gating to a greater extent, and shifted the midpoint of equilibrium inactivation gating to a lesser extent in the mutant channels. The results allow the possibility that an electrostatic mechanism contributes to the role of charged residues in Na channel inactivation gating.

Keywords: *Xenopus* oocyte; Mutagenesis; Patch clamp

1. Introduction

After opening, Na channels quickly close during depolarizing stimuli. Hodgkin and Huxley observed that the rates at which Na channels activate and inactivate both depend on membrane voltage [9,10]. They envisioned activation and inactivation as separate and independent voltage-dependent conformational changes each following first order kinetics. In this regard, the Hodgkin-Huxley model fails to account for later findings that inactivation is delayed relative to activation, that no inactivation gating currents could be recorded, and that once activation has occurred inactivation is uniformly fast and voltage-independent in single channel recordings for most isoforms (reviewed in [29]). These observations led to the current picture of an inactivation process that is not voltage-dependent intrinsically, but rather acquires its voltage dependence by interactive *coupling* with the activation process, which is highly voltage-dependent.

Fig. 1 represents a current view of channel topology, emphasizing the structures responsible for activation and inactivation gating. Movement of the

* Corresponding author. Fax: (804) 9823162;
E-mail: rmoorman@virginia.edu

0005-2736/00/$ – see front matter
PII: S0005-2736(00)00304-7

positively charged S4 segments opens the activation gates [4,16,33,41]. The inactivation gate envisioned by Hodgkin and Huxley is the cytoplasmic linker region between domains III and IV, and this region is thought to swing into a position to occlude the channel pore [34]. This mechanism is roughly homologous to the 'ball and chain' mechanism proposed for N-type inactivation of K channels such as *Shaker* [11].

Although the Na channel III-IV linker and the *Shaker* amino terminal region share little sequence homology, they do share the structural motif of a hydrophobic region lying adjacent to a region with multiple positive charges. In the Na channel III-IV linker the hydrophobic region consists of a cluster of three residues (isoleucine, phenylalanine, and methionine), which are mandatory for fast inactivation [40]. This hydrophobic tripeptide is flanked by a number of highly conserved positive charges. In fact, 12 of the 53 amino acids in the III-IV linker are positively charged and the III-IV linker sequence is highly conserved in multiple species. In *Shaker* K channels both the hydrophobic region and the charged region play important roles, and deletions in both regions disrupt or slow inactivation [11]. Experiments using synthetic ball peptides to reproduce inactivation in inactivation-deficient channels demonstrate that long range electrostatic interactions increase the association rate of the positively charged *Shaker* inactivation ball [22].

Results from mutations of the Na channel III-IV linker suggest an important difference between K channel and Na channel inactivation. Moorman and co-workers replaced small groups of nearby charged amino acids in type III brain Na channels with neutral asparagines, and noted mixed effects [19]. Macroscopic current decay in RNA-injected oocytes was either unchanged or, surprisingly, faster for the mutant channels. Single channel records showed changes in parameters both of activation and inactivation. Catterall and co-workers examined macroscopic currents through similar mutants of type IIA brain Na channel, and saw no effects at all [30]. Currently, electrostatic interactions involving the Na channel inactivation gate are considered unimportant [27], and recent investigations have concentrated on the role of hydrophobic interactions in Na channel inactivation gating [15].

We have reexamined the possible role of positively charged residues in the III-IV linker in Na channel gating. We used site-directed mutagenesis to reduce charge in the III-IV linker, and we measured microscopic and macroscopic currents through oocyte-expressed channels using patch clamp and cut-open oocyte voltage clamp techniques. We have used an approach described by O'Leary and co-workers to diagnose reduced coupling of the activation and inactivation processes [27]. That is, we determined the effect of a channel mutation on the voltage dependence of the inactivation τ_h using Hodgkin-Huxley analysis, and we allow the possibility that the mutated residue is involved in the physical coupling of the two processes if the voltage dependence of τ_h is altered. Despite the acknowledged shortcomings of the Hodgkin-Huxley model, we have found this approach useful in comparing the gating of wild-type and mutant channels.

2. Materials and methods

2.1. Molecular clones

We used the rat skeletal muscle μ1 Na channel, and mutations were made as previously described [21]. To construct the KK 1317/1318 NN mutation, we employed a 55-mer with three base changes using a technique described by Kunkel [17]. The nucleotide mutation resulting in the amino acid changes was AAG AAG 4398–4403 AAC AAC. To select mutants, we simultaneously disabled a *Hin*dIII site at bp 4401–4406 with the nucleotide mutation G 4403 C. To construct the KKK 1322/23/26 NNN mutation, we employed a 60-mer with four base changes. The nucleotide mutations resulting in the amino acid changes were AAG AAG 4413–4418 AAT AAT and AAG 4425–4427 AAC. To select mutations, we employed a fourth base change to introduce a new silent *Bam*HI site by the mutation C 4409 A. All mutations were confirmed by DNA sequencing.

2.2. Oocyte injection

Our methods for oocyte isolation, RNA injection, incubation, and preparation for electrophysiological experiments have been described previously [6,21].

2.3. Patch clamp

Patch clamp electrodes were pulled from capillary glass (Corning 7052) in two stages (Sutter) and heat-polished. The extracellular solution consisted of NaCl 150 mM, KCl 5.4 mM, $CaCl_2$ 1.8 mM, $MgCl_2$ 2 mM, glucose 10 mM, HEPES 10 mM (pH 7.4). The bath solutions, which served as the intracellular solution once the patches were excised, contained K-aspartate 150 (normal ionic strength) or 15 mM (reduced ionic strength), EGTA 10 mM, and HEPES 10 mM (pH 7.4, KOH). A second solution with reduced ionic strength used Cl as the anion. Mannitol was added to the reduced ionic strength solutions to an osmolarity matching the 150 mM K-aspartate solution (300–310 mOsm). Solutions were perfused at a rate of 2–3 ml/min through the 0.5 ml chamber, and were switched using a solenoid device near the chamber. The analog signal was low-pass filtered at 2 kHz (−3 dB) by an Axopatch 200 amplifier (Axon Instruments), then digitized at 20 kHz at 12 bit resolution in pCLAMP.

Cell-attached and excised inside-out patches of mRNA-injected oocytes were obtained at room temperature using conventional means. Capacitance and leak currents were corrected by subtracting the mean of traces without channel activity. Openings were detected using a dI/dt algorithm [37]. The number of channels was taken to be the maximum number of overlapping events at strong depolarization.

2.4. Cut-open clamp

The cut-open oocyte clamp method has been previously described [31,35]. Briefly, defolliculated oocytes were placed in a hole in the floor of a lower perspex chamber, and a Vaseline rim was placed between the oocyte membrane and the edge of the hole. An upper chamber was then positioned so that a second hole corresponded to the upper pole of the oocyte with a second vaseline rim along the edge of the hole. This established three electrically independent compartments with different functions: (a) top pool, which isolated a portion (approx. 25%) of the oocyte membrane; (b) middle pool, for connection to an electronic guard shield; and (c) lower pool, for current injection and access to the oocyte interior. Membrane potential was monitored with a 3 M KCl microelectrode. The lower oocyte membrane was permeabilized by superfusing the intracellular solution with saponin 0.1–0.5%. During saponin superfusion, a square wave potential was applied across the oocyte membrane and the I_m signal capacitative transient was monitored. The lower pool solution was switched to saponin-free intracellular solution when a slow component of the capacitance current appeared. The solution of the middle and lower pools consisted of KCl 120 mM, EGTA 10 mM, HEPES 10 mM (pH 7.4). The solution of the upper pool consisted of NaCl 100 mM, KCl 5 mM, $MgCl_2$ 1 mM, $CaCl_2$ 2 mM, dextrose 10 mM, HEPES 10 mM (pH 7.4). All experiments were performed at room temperature. The current signal was amplified (1 mV/nA, CA-1 oocyte clamp, Dagan Corporation), filtered at 1 kHz (−3 dB, 4-pole low-pass Bessel filter, Dagan), and sampled at 33 kHz (pCLAMP, Axon Instruments). Current records were analyzed using commercial programs (Origin, Microcal; Clampfit, Axon; Excel, Microsoft).

2.4.1. Voltage protocols: equilibrium inactivation and activation

Na currents were elicited by step depolarizations from a holding potential of −120 to test potentials of −50 to 40 mV in 5 mV increments for 30 ms. Currents were corrected for passive components of capacitance and leak currents using a P/n scheme. Each family of corrected current traces was normalized so that the largest current amplitude was 1.0. Normalized currents from multiple experiments were averaged, and the averages were used to construct the current-voltage relationship, the equilibrium activation relationship, and to estimate the time course of current decay.

Equilibrium inactivation was determined using a two-pulse protocol. From a holding potential of −120 mV, a first pulse of varying potential between −110 and 45 mV was delivered for 0.2–1 s. This resulted in inactivation of some proportion of Na channels. The second pulse, to a test potential at or beyond the peak of the IV relationship for 40 ms, was delivered immediately thereafter, and assayed the number of Na channels that did not inactivate. For each oocyte, currents during the second pulse were normalized so that the largest was 1.0,

and results from multiple experiments were averaged.

2.4.2. Voltage protocols: recovery from inactivation

Recovery from inactivation was determined using a two-pulse protocol. The first pulse was from a holding potential of −120 mV to a test potential of 10 mV for 100 ms. This depolarization activated and then inactivated most or all Na channels. After a varying time, a 20 ms pulse to 10 mV was used to assay the proportion of Na channels that had recovered from inactivation. Currents were corrected for passive components of capacitance and leak by subtracting the trace generated at the shortest recovery time, which elicited little or no active Na current. For each oocyte, current amplitudes during this test pulse were normalized so that the largest current when the conditioning potential was −120 was 1.0. The experiment was repeated at conditioning potentials from −120 mV to −80 mV, and results from multiple experiments at the same conditioning potential were averaged.

2.4.3. Voltage protocols: development of inactivation

This was also determined by a two-pulse protocol. The holding potential was −120 mV. The first pulse was of varying duration, and of varying potential from −70 mV to −30 mV. To reset the activation gates without affecting inactivation gating, the membrane potential was returned to −100 mV for 1 ms before the second pulse. The second pulse was to 10 mV for 20 ms. Currents were corrected for passive components of capacitance and leak by subtracting the trace generated with the longest conditioning potential of −70 mV, which generated little or no active Na current. The amplitude of the current during the second pulse was normalized so that the largest was 1.0. Results from multiple experiments at the same first pulse potential were averaged.

2.5. Analysis of single channel dwell times

Frequency histograms of open times and closed times were described with single or sum of two exponentials functions optimized by a maximum likelihood procedure [37]. The sum of two exponentials model was used if the difference in log likelihood compared with the single exponential function exceeded 5. Since channels exhibited bursting behavior, closed time histograms displayed two populations with average dwell times of 1–2 ms and 10–20 ms. We interpreted the short closed times to be closures within bursts and the long closed times to be closures between bursts. We assigned a critical cut-off closed time using the method of Colquhoun and Sakmann [5] that results in equal proportions of errors in assigning closures to within or in-between bursts. The estimated proportion of mis-assignments was 5–20%. Frequencies of histograms of the resulting burst durations were described by single or sum of two exponentials functions, allowing estimation of the proportion of short bursts (usually single openings) and long bursts.

Plots of the cumulative probability of the first opening were described with single or sum of two exponentials functions optimized by a maximum likelihood procedure. The exponential factors were used to calculate the time to half of traces with activity having the first opening. Both this value and the probability of traces with no channel activity were corrected for the number of channels apparent during depolarizations to 0 mV using the method of Horn and co-workers [3]. The average number of wild-type or mutant channels was 2.1–2.5.

2.6. Statistical analysis

2.6.1. Expected values of dwell time and first latency histograms

We represented open time, burst duration and first latency as expected values of exponential functions. Observed frequency histograms of open time and burst duration were described by single or sums of two exponentials functions. Expected values for open time and burst duration were calculated by integrating the fits. First latency distributions were corrected for the number of channels in the patch, which we estimated from the maximum number of overlapping levels at strong depolarizations. We fit the observed first latency distribution to a sum of two exponentials function. Let

$$\mathrm{fl}(t) = A_1 \mathrm{e}^{-\frac{t}{\tau_i}} + A_2 \mathrm{e}^{-\frac{t}{\tau_2}}$$

be the probability distribution function for the first

latency among N channels and let

$$\mathrm{FL}(t) = \int_0^t fl(x)\mathrm{d}x = 1-\left(A_1\tau_1 \mathrm{e}^{-\frac{t}{\tau_1}} + A_2\tau_2 \mathrm{e}^{-\frac{t}{\tau_2}}\right)$$

be its cumulative probability function. Let $p(t)$ and $P(t)$ denote respectively the probability density function and cumulative probability for a single channel. The probability that none of them will have been activated by a time t is $(1-P(t))^N$, so the probability that at least one of them has been activated is $1-(1-P(t))^N = \mathrm{FL}(t)$. To calculate the expected time of activation for a single channel we need $p(t)$. Since

$$P(t) = 1-(1-\mathrm{FL}(t))^{\frac{1}{N}}$$

it follows that

$$p(t) = \frac{\mathrm{d}(P(t))}{\mathrm{d}t} = \frac{\mathrm{fl}(t)}{N}(1-\mathrm{FL}(t))^{\frac{1}{N}-1}$$

Thus the expected time of activation for a single channel is given by

$$\int_0^\infty tp(t) = \frac{1}{N}\int_0^\infty t\left(A_1\mathrm{e}^{-\frac{t}{\tau_1}} + A_2\mathrm{e}^{-\frac{t}{\tau_2}}\right)$$

$$\left(1-\left(A_1\tau_1\mathrm{e}^{-\frac{t}{\tau_1}} + A_2\tau_2\mathrm{e}^{-\frac{t}{\tau_2}}\right)\right)^{\frac{1}{N}-1}\mathrm{d}t$$

2.6.2. Non-parametric multivariate analysis

To test the hypothesis that these mutations altered channel gating, we measured multiple single channel kinetic parameters in three channel types at three test potentials. Usually, differences between channel kinetic parameters are tested individually for statistical significance. If we considered just two kinetic parameters of activation gating, for example, we might thus employ (2)(3)(3) or 18 statistical tests. A potential problem with multiple comparisons is an increased likelihood of type I error, rejecting the null hypothesis when it is in fact true. For example, if a significant difference is concluded for $P<0.05$, then the probability that 18 independent comparisons will yield at least one falsely significant difference is $1-0.95^{18}$, or 0.60. The probability of two or more falsely significant differences (from the binomial distribution) is 0.27. One corrective approach is to adjust the critical value of α from 0.05 to $0.05/n$ where n is the number of tests performed or parameters compared. Loss of power is a major disadvantage of this approach.

We sought a single statistical test that would determine the significance of the differences in gating as measured by multiple parameters among the channel types and voltages. We used a non-parametric multivariate analysis [26]. This is of particular use when the number of measured parameters is large relative to the number of samples, the data are not normally distributed, and prior knowledge allows interpretation of directional trends in the parameter values. The procedure is to assign ranks, adjusted for ties, to a measured parameter for all channel types at a single voltage. For example, rank the mean open times for the three channels for each patch experiment at −40 mV. Repeat the ranking procedure for open times at the other voltages, and for other single channel parameters of interest. Now sum the ranks for each patch. The sum represents the combined information on gating from multiple kinds of measurements. These data can be tested by one-way ANOVA if the question is whether the channels differ at any one voltage. Since we had data from three voltages, we extended the technique to two-way ANOVA to yield an approximation of the P-value.

2.6.3. Limitations

Measurements from the same patch at different voltages are included. This is advisable only if the measurements are not influenced by the history of the experiment. We do not know whether gating at one voltage is influenced by prior depolarizations to other voltages, and allowing replication may limit these particular results. For this work, we operationally defined fast activation as short first latency and few traces without openings, and we defined fast inactivation as short open time and short burst duration. This selection is arbitrary, but the general method should be applicable to evaluation of models of single channel gating in which unambiguous prediction of the behavior of groups of kinetic parameters is possible.

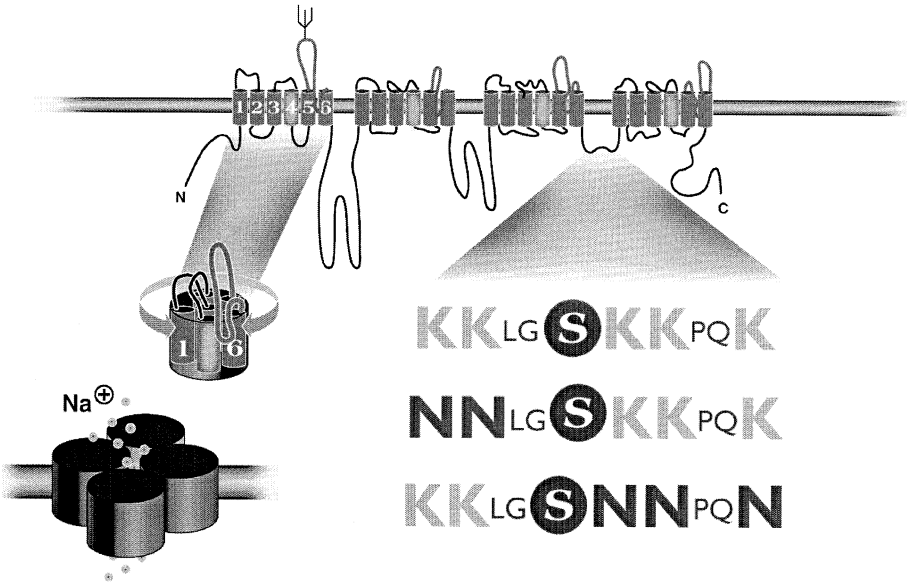

Fig. 1. Na channel topology and molecular clones used in the study. Four heterologous domains, each consisting of six transmembrane segments, are connected by cytoplasmic linkers. A proposed folding scheme is shown on the left, and the result is a transmembrane structure surrounding an aqueous pore through which sodium ions permeate. The focus of this work is the cytoplasmic linker region between domains III and IV. The three amino acid sequences on the right are from the 53 highly conserved amino acids of the linker. The first set is the wild-type sequence; the second is the KK 1317/18 NN mutant sequence; the third is the KKK 1322/23/26 NNN mutant sequence. Ks are positively charged lysine residues and Ns are the uncharged but otherwise conservative substitute asparagines.

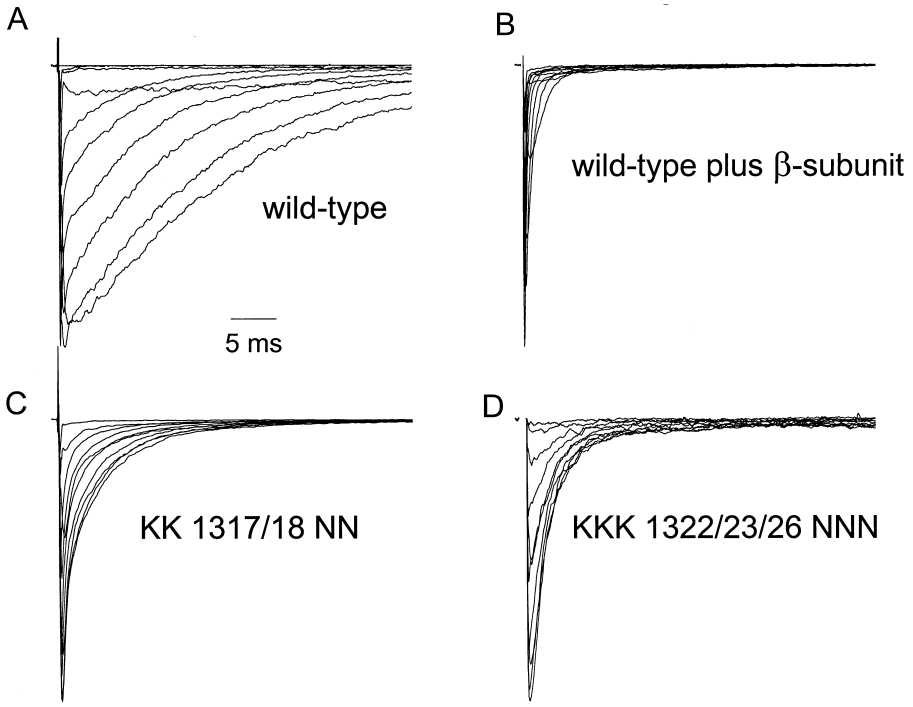

Fig. 2. Macroscopic current decay is faster through mutant Na channels. (A–D) Families of Na currents in RNA-injected oocytes elicited from a holding potential of −100 mV to test potentials from −50 to 50 mV in 5 mV increments using the excised inside-out patch clamp technique. Data are from one oocyte in each panel. Current amplitudes have been normalized. Note that current decay is faster for the mutant channels.

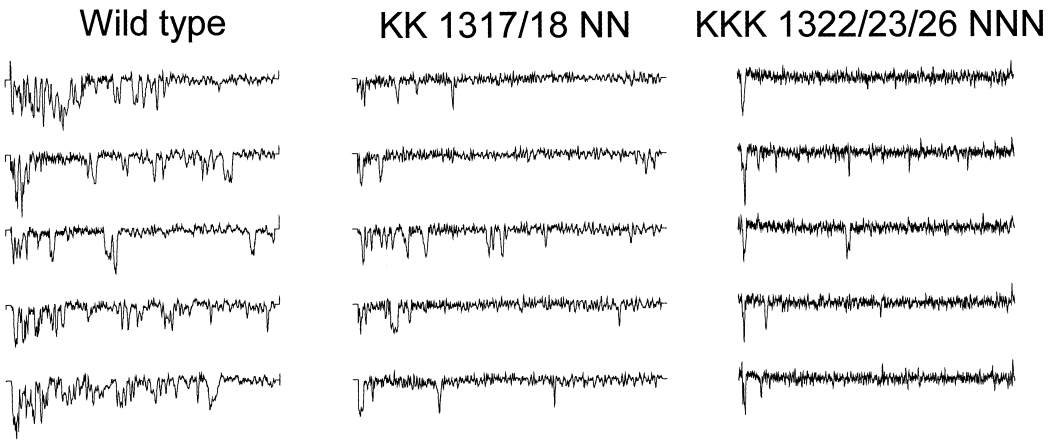

Fig. 3. Representative single Na channel currents in cell-attached patches at −20 mV. Shown are five consecutive single channel recordings produced by 100 ms depolarizations from a holding potential of −100 mV to a test potential of −20 mV in cell-attached patches from oocytes expressing wild-type, KK 1317/18 NN, and KKK 1322/23/26 NNN channels. The scale bars are 5 ms and 2 pA.

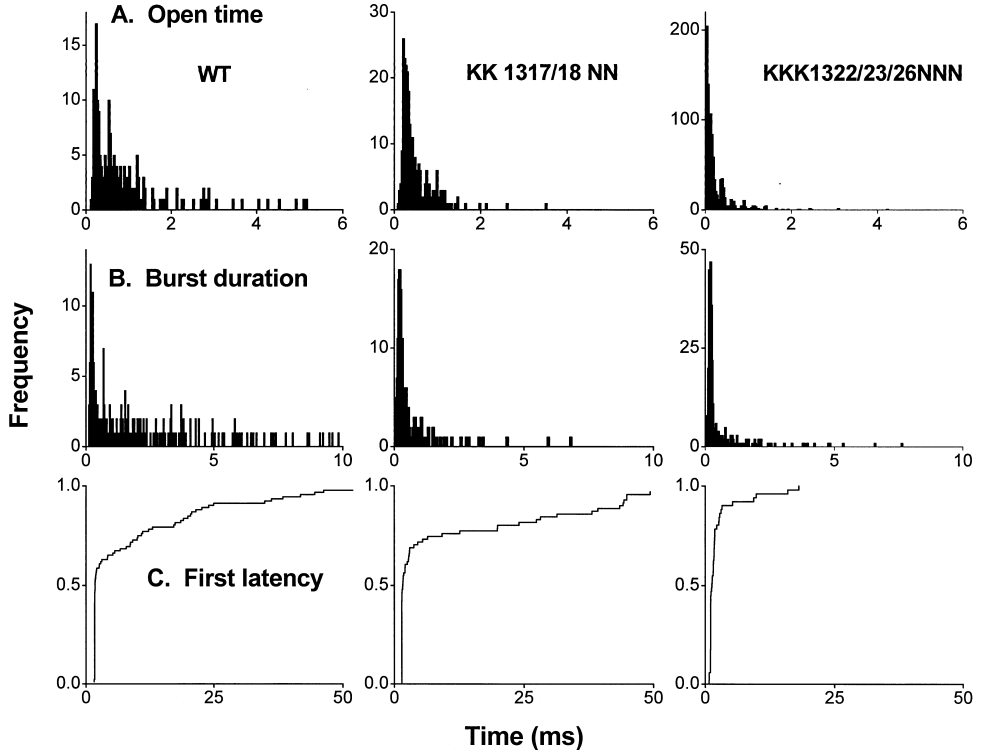

Fig. 4. Effect of K to N substitutions on channel dwell times and first latencies. Representative open time histograms (A), burst duration histograms (B), and first latency distributions (C) are shown for wild-type μ1, KK 1317/18 NN, and KKK 1322/23/26 NNN channels at a test potential of 0 mV. Both mutant channels have fewer long openings or long bursts (A,B). KKK1322/23/26 NNN channels also had shorter first latencies (C).

3. Results

3.1. Do mutant KK 1317/18 NN and KKK 1322/23/26 NNN channels have altered activation and inactivation kinetics?: macroscopic currents in cell-attached patches

Fig. 1 shows the wild-type sequence (top) and the two mutant sequences KK 1317/18 NN (middle) and KKK 1322/23/26 NNN (bottom). The effect of each is to reduce positive charge near the conserved serine that is a PKC phosphorylation site (circled) [23,39]. Fig. 2 shows currents through wild-type and mutant Na channels in exemplary excised inside-out patches. An obvious difference is the more rapid decay of currents through mutant KK 1317/18 NN and KKK 1322/23/26 NNN channels. Fig. 2A shows the anomalously slow decay of currents through channels comprised of α-subunits alone, and Fig. 2B shows the effect of co-expressed β-subunit to speed decay. Both kinds of mutant channels showed faster decay kinetics (Fig. 2C,D), similar to the mutations of the type III rat brain Na channel [19] and the deletion of the nearby KPQ sequence of cardiac Na channels in one variant of the long QT syndrome [1].

3.2. Do mutant KK 1317/18 NN and KKK 1322/23/26 NNN channels have altered activation and inactivation kinetics?: microscopic currents in cell-attached patches

Single channel analysis of the type III rat brain mutant channels showed alterations in both activation and inactivation gating [19]. Fig. 3 shows representative current recordings during depolarizations

Table 1
Single channel gating analysis

	Open time (ms)		
	−40 mV	−20 mV	0 mV
Wild-type	0.57 ± 0.09	0.88 ± 0.1	1.02 ± 0.2
KK 1317/18 NN	0.77 ± 0.1	0.84 ± 0.08	0.66 ± 0.04
KKK 1322/23/26 NNN	0.75 ± 0.1	0.40 ± 0.05	0.49 ± 0.08
	Burst duration (ms)		
	−40 mV	−20 mV	0 mV
Wild-type	0.89 ± 0.1	1.99 ± 0.2	3.23 ± 0.7
KK 1317/18 NN	1.40 ± 0.2	1.65 ± 0.2	1.16 ± 0.1
KKK 1322/23/26 NNN	0.87 ± 0.3	1.69 ± 0.4	1.82 ± 0.6
	Expected first latency (ms)		
	−40 mV	−20 mV	0 mV
Wild-type	41.4 ± 1.6	28.1 ± 1.1	37.6 ± 1.8
KK 1317/18 NN	50.3 ± 1.7	32.2 ± 1.2	38.1 ± 1.3
KKK 1322/23/26 NNN	33.2 ± 2.3	29.6 ± 1.0	13.4 ± 1.6
	Proportion of null traces		
	−40 mV	−20 mV	0 mV
Wild-type	0.78 ± 0.01	0.47 ± 0.01	0.39 ± 0.01
KK 1317/18 NN	0.59 ± 0.01	0.32 ± 0.008	0.37 ± 0.01
KKK 1322/23/26 NNN	0.48 ± 0.04	0.32 ± 0.009	0.23 ± 0.01

Parameters were derived from multiple patches as described in the text. For wild-type channels, 16 patches were studied at −40 mV, 19 patches at −20 mV and 14 patches at 0 mV. For KK 1317/18 NN channels respectively 21, 25 and 17 patches were studied at each potential and for KKK 1322/23/26 NNN channels respectively 14, 15 and 14 patches were studied at each potential. 100 sweeps were analyzed for each patch. The numbers of wild-type channels (mean, S.E.) per patch were 2.2, 0.3 (0 mV), 2.2, 0.3 (−20 mV) and 2.2, 0.3 (−40 mV). The numbers of KK 1317/18 NN channels per patch were 2.4, 0.4 (0 mV), 2.4, 0.4 (−20 mV) and 2.60, 0.3 (−40 mV). The numbers of KKK 1322/23/26 NNN channels per patch were 2.2, 0.2 (0 mV), 2.2, 0.2 (−20 mV) and 2.2, 0.2 (−40 mV).

to a test potential of −20 mV for wild-type μ1, KK 1317/18 NN, and KKK 1322/23/26 NNN channels. Qualitatively, the mutations produced mixed single channel effects. Records from mutant channels had fewer null traces and fewer late openings, and these findings were more apparent in the KKK 1322/23/26 NNN mutant channels.

For quantitative analysis, we measured multiple single channel kinetic parameters in the three channel types at three test potentials. Fig. 4 shows representative dwell time histograms and first latency distributions for the channels at a test potential of 0 mV. The histograms were fit to a sum of two exponentials function. We used the exponential fits to calculate expected values for open time, burst duration, and first latency. Values were corrected for the estimated number of channels in each patch. Table 1 lists the expected values for open time, burst duration, and first latency as well as the proportion of null traces. The mutations had effects on both activation and inactivation parameters. First, both open time and burst duration were shorter for the mutants at strong depolarizations, especially for KKK 1322/23/26 NNN. Second, first latency of the KKK 1322/23/26 NNN mutant at a test potential of 0 mV was dramatically shorter than for the other channels. Third, the proportion of null traces was reduced for the mutant channels.

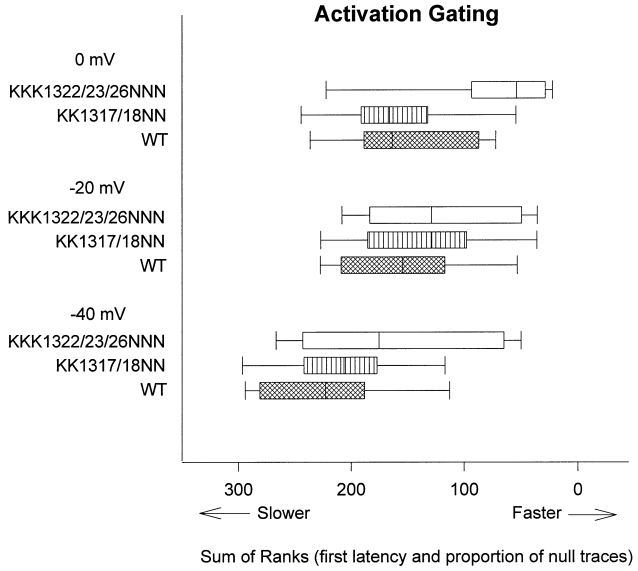

Fig. 5. Box plots of multivariate rank sum analysis of activation gating. The data symbols are the sum of ranks for first latency and proportion of nulls. In the box plot symbol, the enclosed vertical line is the median, the box encloses 50% and the hatches enclose 80% of the data points. Boxes to the right reflect faster channel activation gating. Data represent measurements from 13–25 patches, 100 sweeps/patch. The major finding is that KKK 1322/23/26 NNN channels have faster activation gating than wild-type or KK 1317/18 NN channels at 0 mV.

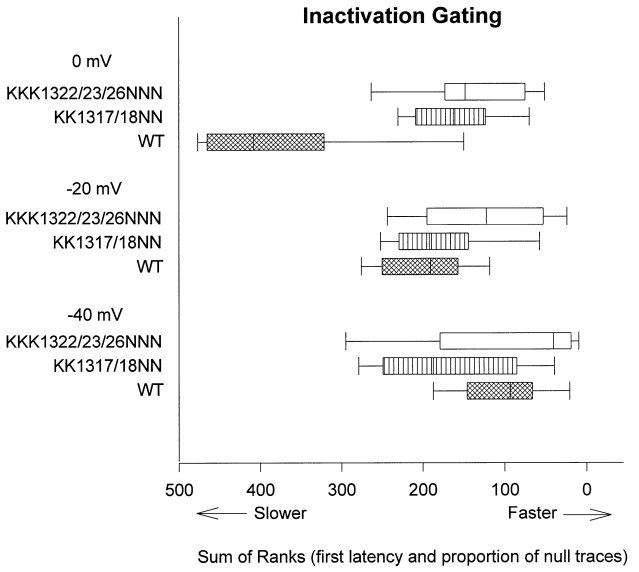

Fig. 6. Box plots of multivariate rank sum analysis of inactivation gating. The data symbols are the sum of ranks for open time and burst duration. Boxes to the right reflect faster channel inactivation gating. Data represent measurements from 13–25 patches, 100 sweeps/patch. The major findings are (1) KKK 1322/23/26 NNN channels have faster inactivation gating than wild-type or KK 1317/18 NN channels at test potentials of −20 and 0 mV and (2) KK 1317/18 NN channels have faster inactivation gating than wild-type at test potential 0 mV.

Box plots of the sums of ranks for each channel at the three test potentials are shown in Fig. 5 for the activation parameters and in Fig. 6 for the inactivation parameters. To maximize the statistical power of multiple measurements and at the same time avoid type I error, we employed a non-parametric multivariate analysis that minimized the number of statistical comparisons [26]. At a test potential of 0 mV, the KKK 1322/23/26 NNN mutation accelerated both activation and inactivation gating, and the KK 1317/18 NN mutation accelerated inactivation gating. At test potentials of −20 and −40 mV, the differences were progressively less marked. Overall, two way ANOVA indicated significantly faster activation and inactivation gating for the KKK 1322/23/

26 NNN mutant compared to the other two channels ($P < 0.001$ for activation gating and $P = 0.003$ for inactivation gating). The effects were voltage-dependent with least difference at −40 mV and increasing effect at the stronger depolarizations.

3.3. Do mutant KK 1317/18 NN and KKK 1322/23/26 NNN channels have altered activation and inactivation kinetics?: macroscopic currents in cut-open oocytes

Fig. 7A–C show families of Na currents during depolarizing steps in cut-open oocytes expressing wild-type and mutant Na channels. Fig. 7D shows the initiation of superimposed currents at a test potential of −10 mV. The current amplitudes have been normalized to emphasize the large difference in decay kinetics, which were quantified using sums of two exponentials functions. The current through mutant KK 1317/18 NN channels had a fast τ of 1.5 ms accounting for 87% of the initial amplitude compared with 2.6 ms and 72% for the current through wild-type channels. The current through mutant KKK 1322/23/26 NNN channels decayed faster still, with a time constant of 0.90 ms accounting for 96% of the initial amplitude. Since activation is rapid (especially in the KKK 1322/23/26 NNN channels) and complete or nearly complete at this test potential, these faster time constants can be interpreted as estimates of the rate of fast inactivation. These fast decay τs are shown as a function of voltage in Fig. 7E. Currents through mutant channels decayed more

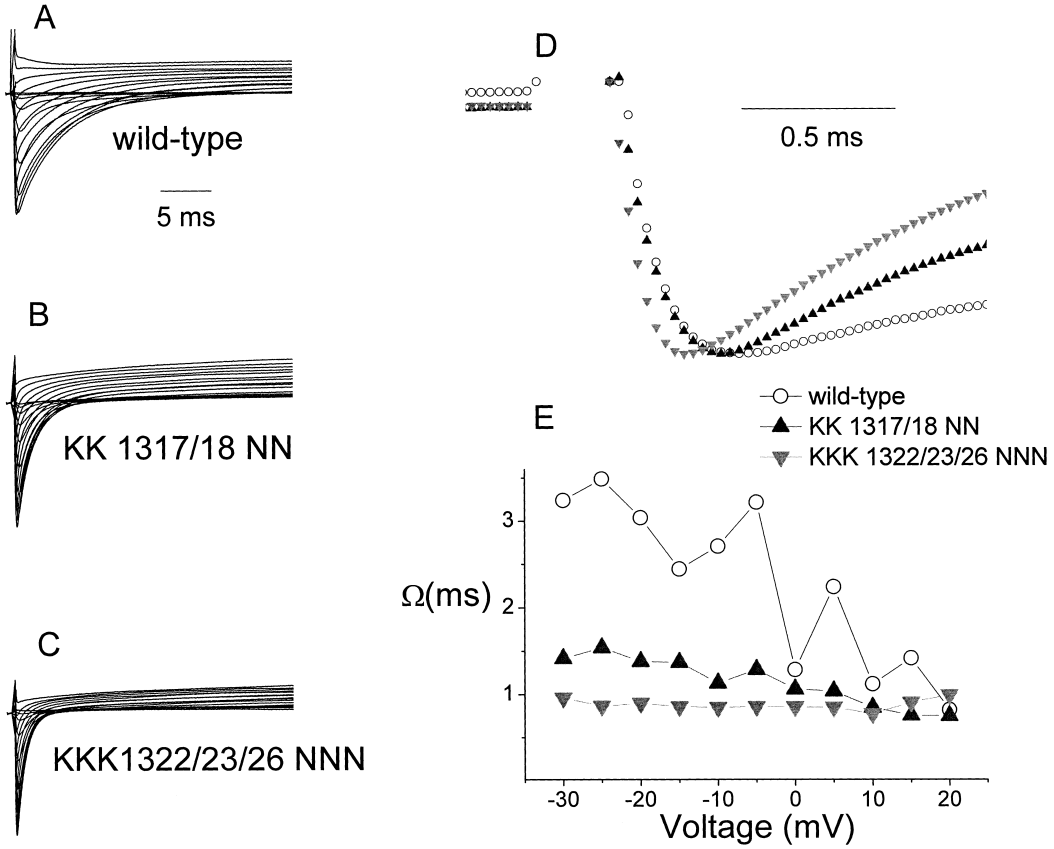

Fig. 7. Families of Na currents in RNA-injected *Xenopus* oocytes elicited from a holding potential of −100 mV to test potentials from −50 to 50 mV in 5 mV increments using cut-open oocyte voltage clamp technique. Averages of 15–25 recordings; current amplitudes have been normalized. (D) Superimposition of initial normalized currents on an expanded time scale at a test potential of −10 mV. (E) The decay phases of macroscopic currents were fit with a sum of two exponentials model:

$$I_t = A_0 + A_1\exp(-t/\tau_1) + A_2\exp(-t/\tau_2)$$

The fast decay τ as a function of voltage is shown as panel E.

quickly and, whereas currents through wild-type channels decayed more quickly with larger depolarizations, the decay kinetics for the mutant channels were independent of voltage.

The finding of more rapid decay of Na channels with K to N mutations in the inactivation gate are in agreement with earlier findings for the type III rat brain Na channel analog of the KKK 1322/23/26 NNN mutation [19]. In that study, no currents could be measured in oocytes injected with the analog of the KK 1317/18 NN mutant channel RNA. These large differences in decay kinetics suggest that charged residues play a role in Na channel inactivation gating, and we proceeded to measure equilibrium gating properties and inactivation time constants across a wider voltage range.

3.4. Equilibrium properties were different for mutant channels

Fig. 8A shows the current-voltage relationships, and Fig. 8B shows the equilibrium activation and inactivation relationships. In the latter, the smooth lines are the fits to Boltzmann functions. The parameters are given in Table 2. The slope factors for all three kinds of channels are very similar, suggesting that the voltage sensitivity of equilibrium gating properties is not changed by the charge-reducing mutations. The midpoints, however, are different. The midpoint of the equilibrium inactivation relationship for the KKK 1322/23/26 NNN channels was shifted about 10 mV in the hyperpolarizing direction while that of the KK 1317/18 NN channels was shifted about 2.5 mV in the depolarizing direction. By two-way ANOVA of the available peak currents between conditioning potentials of −90 and −50 mV,

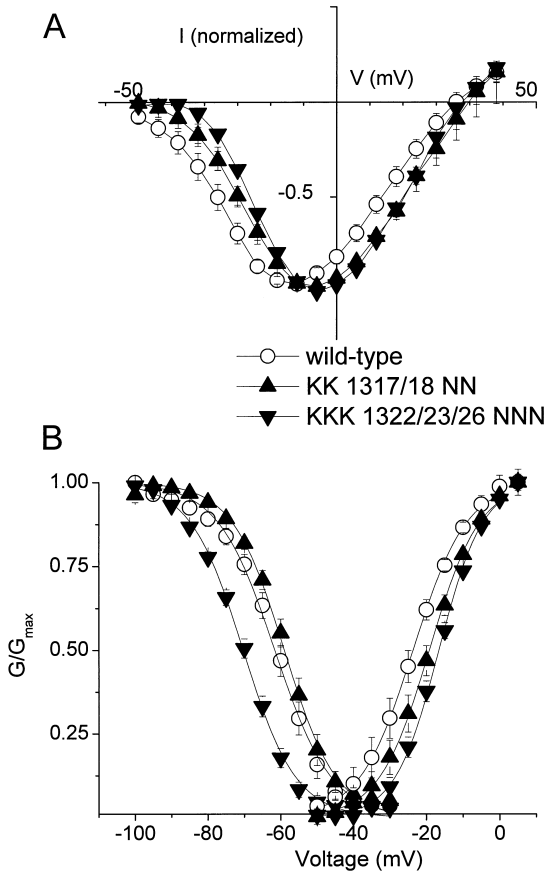

Fig. 8. Equilibrium properties of activation and inactivation. (A) Peak current-voltage relationships. (B) Equilibrium inactivation and activation relationships. The smooth lines are Boltzmann functions of the form

$$\frac{G}{G_{\max}} = \frac{1}{1+\frac{V-V_{0.5}}{k}}$$

where $V_{0.5}$ is the voltage at which half the channels are activated or inactivated at equilibrium, and k is a slope factor equal to RT/zF where z is the number of charges that move during the conformational transition. Data points are the average of 15–25 recordings; bars are S.E.M.

Table 2
Equilibrium parameters of Na channel gating in cut-open oocytes

	Inactivation			Activation		
	$V_{0.5}$ (mV)	k	n	$V_{0.5}$ (mV)	k	n
Wild-type	−61.59 ± 1.32	−7.50 ± 0.68	9	−23.65 ± 0.32	6.1 ± 0.08	17
KK 1317/18 NN	−58.97 ± 1.14	−6.9 ± 0.42	6	−19.20 ± 0.31[a]	6.42 ± 0.07	15
KKK 1322/23/26 NNN	−70.39 ± 0.39[a]	−6.9 ± 0.21	14	−16.60 ± 0.14[a]	5.65 ± 0.03	25

Values of $G/G_{\max}$ from individual determinations were fit to Boltzmann functions.
[a]Significantly different from wild-type by ANOVA.

the KKK 1322/23/26 NNN channels were significantly different from the other two.

Both kinds of mutant channels showed a depolarizing shift of the midpoint of the equilibrium activation relationship, by about 4.5 mV for KK 1317/18 NN channels and by about 7 mV for KKK 1322/23/26 NNN channels. By two-way ANOVA of the peak currents between test potentials of −40 and −5 mV, each channel was significantly different from the other two. One interpretation of these findings is that the voltage sensor of each channel detects a different electrical field strength. Specifically, the rightward shift of the equilibrium activation relationship is compatible with the idea that the voltage sensors of the mutant channels sense less positive charge. Stuhmer and co-workers [33] suggested that the midpoint of the equilibrium activation relationship is a gauge of the electrical field sensed by the voltage-sensing S4 segments. In their work, a finding of a shift to depolarized potentials reflects a reduction in the positive charge near the intracellular face of the voltage sensor. Our results might be similarly explained if this charged region of the III-IV linker is within the electrical field of the voltage-sensing S4 segments. This is re-addressed below in the description of experiments where the ionic strength of the intracellular solution was varied.

3.5. The voltage dependence of inactivation was altered in the mutant channels

To determine the voltage dependence of inactivation across a wide range of potentials, we measured the time courses of recovery from and development of inactivation in cut-open oocytes and fit the averaged data to sums of exponentials function. We called the fast time constants τ_{rec} and τ_c, respectively, and refer to them together as τ_h. Fig. 9 shows inactivation kinetics (τ_{rec}, open and τ_c, crossed symbols) and equilibrium values (filled symbols) as a function of voltage for wild-type (Fig. 9A), KK 1317/18 NN (Fig. 9B) and KKK 1322/23/26 NNN (Fig. 9C) channels. Inactivation kinetics were consistently faster at all voltages in the mutant channels. We examined these relationships for evidence of uncoupling of the processes of activation and inactivation. The tests we applied were (1) measuring the dynamic range of τ_h, where reduced range signifies reduced voltage de-

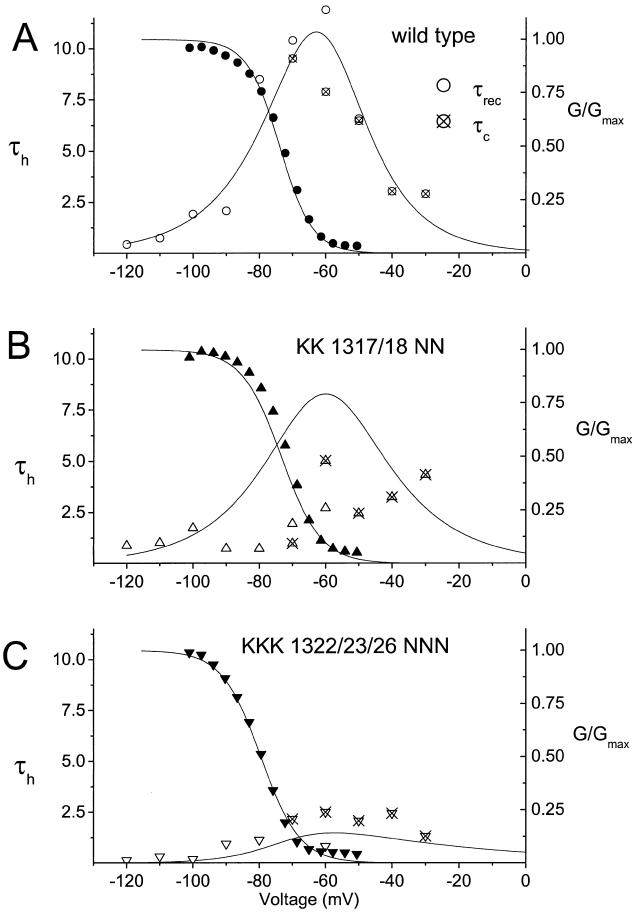

Fig. 9. Equilibrium and kinetic properties of inactivation. Each plot shows the averaged h_∞ data from Fig. 8 (filled symbols), τ_{rec} (open symbols), and τ_c (crossed symbols) for wild-type (A), KK 1317/18 NN (B), and KKK 1322/23/26 NNN (C) Na channels. Inactivation τ_h was faster at all potentials for both mutants. The smooth lines are fits to:

$$\text{steady} - \text{state inactivation} = \frac{\alpha_h(V)}{\alpha_h(V) + \beta_h(V)}$$

$$\tau_h = \frac{1}{\alpha_h(V) + \beta_h(V)}$$

$$\alpha_h(V) = \alpha_h^0 \exp -(z - \delta z)FV/\mathrm{RT}$$

$$\beta_h(V) = \beta_h^0 \exp(\delta z)FV/\mathrm{RT}$$

where δ is a factor of asymmetry that gives the fractional influence of V on the gating particle, z is the equivalent charge of the gating particle, and $F/\mathrm{RT} = 0.04$ mV. Values of α, β, δ, and z were determined by minimization of squared errors (Excel, Microsoft).

pendence, and (2) estimating the goodness of fit of Hodgkin-Huxley theory to the results, where a poor fit signifies a departure from the assumption that a single conformational transition underlies the inactivation process [27].

First, we observed reduced voltage dependence of τ_h for the mutant channels. τ_h varied within a smaller dynamic range for KK 1317/18 NN (about 18-fold) and KKK 1322/23/26 NNN (about 16-fold) channels compared with wild-type (about 30-fold).

Second, we fit the data to the Hodgkin-Huxley model. A central assumption in using this model to interpret these kinds of data is that the rate-limiting step in Na channel inactivation is a single conformational transition that follows first order kinetics. If that assumption does not hold, then plots of inactivation kinetics at equilibrium as a function of voltage will not be fit by Hodgkin-Huxley equations [27].

The results are shown as smooth lines in Fig. 9. To determine the goodness of fits to theory, we calculated χ^2 for ten values of τ_h in each plot. The values were 0.22 (wild-type), 3.45 (KK 1317/18 NN) and 2.44 (KKK 1322/23/26 NNN). For 8 degrees of freedom, the two-tailed probabilities that the fits are due to chance are $\ll 0.0005$, 0.10 and < 0.05, respectively. Hence the wild-type data were substantially better fit by theory than either of the mutants, and KK 1317/18 NN channels were not fit at all.

3.6. Could electrostatic changes contribute to the gating effects?: macroscopic currents in excised inside-out patches

The findings above demonstrated that neutralization of positively charged residues altered activation and inactivation gating, and the coupling of inactivation to activation. The shift of the equilibrium activation relationship for the mutant channels allowed the possibility of an electrostatic mechanism. We further tested the possibility of an electrostatic interac-

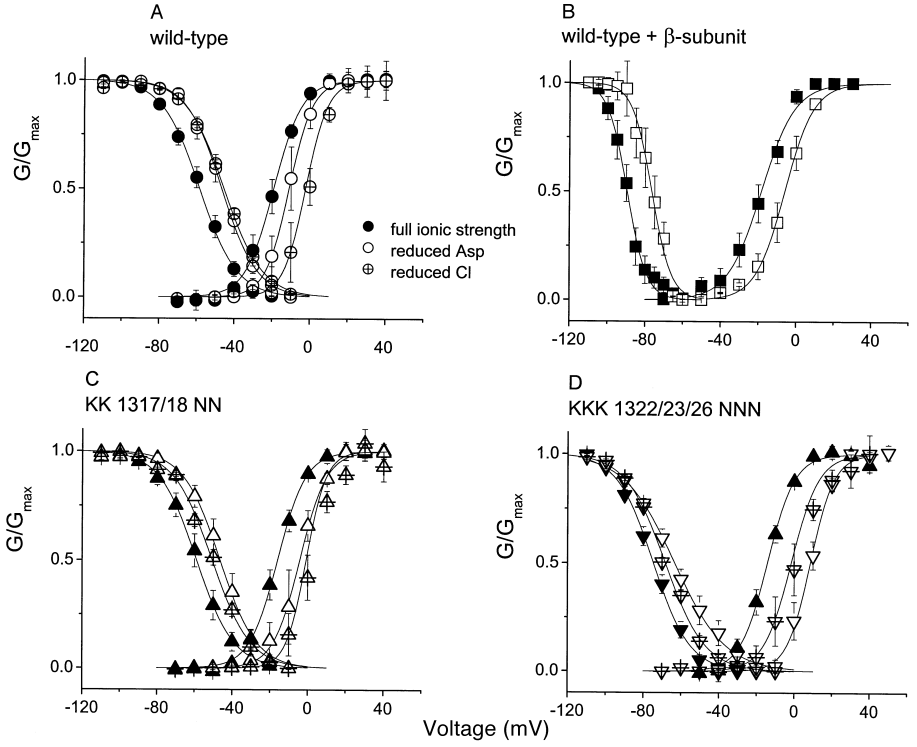

Fig. 10. Reducing ionic strength alters equilibrium properties of activation and inactivation. Equilibrium inactivation and activation relationships in full ionic strength (closed symbols) and reduced ionic strength (open symbols) solutions for wild-type (A), KK 1317/18 NN (B), and KKK 1322/23/26 NNN (C) channels. The smooth lines are Boltzmann functions. Data points are the mean of 5–15 patches with macroscopic current; bars are S.E.M. The changes were readily reversible and could be demonstrated repeatedly in the same patch. Full ionic strength solutions contained 150 mM aspartate. Low ionic strength solutions contained 15 mM aspartate or 15 mM Cl.

Table 3
Equilibrium gating parameters in excised patches

	Full ionic strength			Reduced ionic strength (Asp)			Reduced ionic strength (Cl)		
	$V_{0.5}$ (mV)	k	n	$V_{0.5}$ (mV)	k	n	$V_{0.5}$ (mV)	k	n
Inactivation									
Wild-type	−58.2 ± 2.1	−9.0 ± 0.3	13	−46.7 ± 2.5**	−8.7 ± 0.3	6	−45.2 ± 2.6	9.3 ± 0.3	8
Wild-type plus β-subunit	−89.2 ± 2.2*	−5.7 ± 0.4	6	−77.1 ± 3.2*,**	−5.3 ± 0.3	6			
KK 1317/18 NN	−59.2 ± 3.1	−7.7 ± 0.3	14	−46.5 ± 3.0**	−8.3 ± 0.5	8	−50.3 ± 3.5	8.4 ± 0.3	7
KKK 1322/23/26 NNN	−74.6 ± 1.9*	−9.1 ± 0.24	12	−63.3 ± 3.8*,**	−10.6 ± 0.8	6	−67.9 ± 1.9	10.3 ± 1.2	6
Activation									
Wild-type	−20.0 ± 2.0	5.6 ± 0.3	12	−14.2 ± 0.8**	5.2 ± 0.4	6	−1.7 ± 2.8**	5.9 ± 07	5
Wild-type plus β-subunit	−21.5 ± 1.4	7.6 ± 0.2	13	−11.2 ± 1.1**	6.6 ± 0.4	8			
KK 1317/18 NN	−16.1 ± 1.7*	5.7 ± 0.2	13	−5.4 ± 3.0*,**	5.3 ± 0.2	6	0.1 ± 2.5**	5.4 ± 0.7	5
KKK 1322/23/26 NNN	−13.7 ± 1.2*	6.0 ± 0.2	15	6.5 ± 1.7*,**	4.7 ± 0.4	9	−2.1 ± 3.7**	6.3 ± 0.7	5

Values of G/G_{max} from individual determinations were fit to Boltzmann functions. Full ionic strength solutions contained 150 mM aspartate; reduced ionic strength solutions contained 15 mM aspartate (Asp) or 15 mM Cl.
*$P < 0.05$ for the comparison with wild-type channels by ANOVA.
**$P < 0.05$ for the comparison of solutions of full and reduced ionic strength by t-test.

tion of the III-IV linker and the voltage-sensing S4 segments by measuring equilibrium gating properties in an intracellular solution with reduced ionic strength. This condition reduces the number of counterions available to shield the charge of amino acids and membrane lipids. All equilibrium properties will shift in the depolarizing direction, consistent with a more pronounced electrical field of the now unshielded negatively charged regions of the channel protein that contribute to the membrane surface potential. If the charged residues involved in the mutations reside within the electrical field of the voltage sensor, then reducing ionic strength should have a disproportionately large effect on the voltage dependence of gating properties for the mutant channels.

Fig. 10 shows the equilibrium activation and inactivation relationships for the wild-type and mutant channels. In addition, we performed these experiments on oocytes co-expressing wild-type α-subunits and the brain β-subunit. The smooth lines are the fits to Boltzmann functions, and the parameters are given in Table 3. These experiments confirmed the significant rightward shifts of equilibrium activation for the mutant channels noted in the cut-open oocyte experiments ($P < 0.05$, two-way ANOVA). The substantial leftward shift of equilibrium inactivation for KKK 1322/23/26 NNN was affirmed in these experiments. As previously reported, co-expression of β-subunit led to a hyperpolarizing shift of equilibrium inactivation [12].

Fig. 10 also shows the results in intracellular solutions with reduced ionic strength. The coupling between activation and inactivation leads to the expected finding of parallel shifts in equilibrium gating, but the degree of shift differs for activation and inactivation. For example, in wild-type channels we found a shift in the midpoint of activation gating from −20.0 mV to −14.2 mV, and a shift in the midpoint of inactivation gating from −58.2 mV to −46.7 mV under conditions of reduced ionic strength in which Asp was the anion. The ratio of the shifts in activation gating to inactivation gating is (−20.0–(−14.2)) mV/(−58.2–(−46.7)) mV, or 0.5 mV/mV. This is similar to the reported 0.7 mV/mV shift for the cardiac hH1 Na channel isoform compared with the skeletal muscle μ1 isoform [24,25,38], and underscores the importance of the coupling process. The important finding is that the mutant channels showed larger changes in activation gating relative to inactivation gating than wild-type. The ratios were 0.8 ± 0.06 mV/mV for KK 1317/18 NN channels and 1.1 ± 0.06 mV/mV for KKK 1322/23/26 NNN channels. The latter was significantly different from wild-type ($P < 0.05$, ANOVA). When a reduced ionic strength solution in which Cl was the anion was used, a similar trend was observed (1.4 ± 0.1 mV/mV in wild-type channels, 1.8 ± 0.2 mV/mV in KK 1317/18 NN channels, and 1.7 ± 0.03 mV/mV in KKK 1322/23/26 NNN channels). The difference in the results in the Asp solution compared with the Cl solu-

tion is not explained, but might relate to the difference in sizes of the anions.

4. Discussion

We have studied the effect on Na channel gating of positively charged residues in the inactivation gate. Our approach was to characterize gating in two mutant channels with charge neutralization by asparagine substitution for lysines. The major findings for the mutant channels were (1) the time constants of fast inactivation were faster at all potentials, (2) inactivation was less well coupled to activation, (3) the midpoints of equilibrium inactivation and activation gating were shifted, and (4) reducing intracellular ionic strength had different effects than for wild-type channels. Overall, the findings suggest a role for positively charged residues in the III-IV linker in Na channel gating.

Recent studies have identified naturally occurring and site-directed Na channel mutations that alter activation-inactivation coupling [3,4,14,27,32,36]. These mutagenesis studies all suggest that charge displacement during activation may translate through some physical, molecular link into conformational changes in the inactivation gating mechanism. Details of the mechanism of this linkage remain unclear, and as yet there is no compelling model that synthesizes all the data. We propose a qualitative model in which this coupling is due, at least in part, to repulsion of the positively charged III-IV linker and the like-charged S4 segments.

The model is predicated on (1) the presence of S4 positive charges near the cytoplasmic face of the channel molecule when it is closed, and (2) a reduction in this charge density after the S4 segments move during channel opening. We speculate that this charge density of the closed channel might serve to repel the positively charged III-IV linker. When the S4 segments move away during channel opening, the charged linker is allowed to relax toward the channel pore. This may be driven by the hydrophobic interactions of the IFM segment with its receptor that lead to the inactivated state.

Several predictions follow from this model. First, if removing positive charges from the inactivation gate reduces electrostatic repulsion, inactivation of the mutants should be faster at all voltages. Second, removing charges should weaken the coupling of activation and inactivation, and the mutant channels should fail to be described by the Hodgkin-Huxley model [27]. Both predictions are met, as demonstrated in Fig. 9. Third, the inactivation gate must lie within the electrical field of the voltage sensor, and thus reduction of charge in the inactivation gate should shift the midpoint of the equilibrium activation relationship to depolarized potentials. In both the cut-open oocyte preparation and in excised inside-out patches with cytoplasmic solution of full ionic strength, both mutant channels showed such shifts. Fourth, channel gating should be sensitive to changes in ionic strength. Accordingly, we measured equilibrium properties of activation and inactivation in conditions of reduced ionic strength. If the mutated residues are within the electrical field of the voltage sensor, then the effect of the reduced ionic strength solution will differ from that of the wild-type channels. The main finding was that reduced ionic strength solution shifted the midpoint of equilibrium activation more for mutant than for wild-type channels.

Another finding was that the midpoint of the equilibrium inactivation relationship, which should passively follow the equilibrium activation relationship, shifted less than expected in the mutant channels. This was demonstrated in the increased ratio of the shift in midpoint of activation gating to the shift in midpoint of inactivation gating, from 0.5 mV/mV in wild-type channels to 0.8 and 1.1 mV/mV in the KK 1317/18 NN and KKK 1322/23/26 NNN channels, respectively. If the change in ionic strength affects only the surface potential, then equilibrium activation and inactivation parameters should shift equally [8]. One possible interpretation of the different amount of the shifts is that the charge-reducing mutations altered an interaction of channel structures that contributed to the coupling.

The model would also predict that substitution of negatively charged residues into positions 1317, 1318, 1322, 1323 and/or 1326 should speed inactivation and reduce the apparent coupling of activation and inactivation even more than the neutral residues that we have chosen. The model would predict that increasing intracellular ionic strength would undo the effect of these charge reduction mutations.

These predictions should serve as future tests of these ideas.

4.1. Relationship to past work

Like reduction of charge in the inactivation gate, reduction of charge in the S4 segments near the intracellular face of Na [33] and K [18,28] channels also shifts the midpoint of equilibrium activation to depolarized potentials. This was first demonstrated for charges in S4 segments of domains I and II of the rat brain type II Na channel. An extreme example was the KKK 226/859/862 QQQ mutant, which showed a 43 mV shift. Interestingly, that mutant also displayed a 22 mV hyperpolarizing shift of equilibrium inactivation. Both findings are similar to those in the mutant channels reported here. Since a reduction in charge in either the intracellular aspects of the S4 segments or in the III-IV linker led to the same changes, it is attractive to speculate that the charges reside in the same electrical field.

4.2. Limitations and alternative explanations

The Na channel β-subunit, which increases the proportion of channels in the fast gating mode [2,12], was not used in all of the experiments. The goal, however, was to isolate the effect of changing the charge of the α-subunit inactivation gate. We have focused on the fastest time constants of inactivation, which are not changed by β-subunit co-expression. One of the most important findings – altered shifts of equilibrium gating parameters when intracellular ionic strength was reduced – was not affected by the presence of the β-subunit (Fig. 10). A related uncertainty is the effect of the mutations on the voltage-dependent fast and slow modes of Na channel gating [13,20,42]. Further studies of single channel kinetics are required to address this issue.

We combined single channel kinetic parameters to compare activation and inactivation processes. While this approach achieved the statistical goal of minimizing the number of comparisons and thus increasing the power of the analysis, it came at the cost of assumptions about channel gating. For example, we view the first latency as a measure of activation but it might also reflect channel inactivation. For example, the proportion of null traces or the elimination of a slow component from the first latency histogram might indicate an acceleration of closed channel inactivation rather than an acceleration of activation. This kind of uncertainty is present in interpreting single channel gating kinetic data, and the new statistical approach is also prey to it.

We modified intracellular ionic strength by using low K-aspartate and low KCl solutions made isoosmotic with mannitol. Another approach would have been to use divalent or trivalent ions. Since the electrostatic potential of an ion in solution is an exponential function of the valence, this would have given us greater impact on surface potential. Their use, however, is complicated by the possibility of binding or other interaction with channel proteins.

There are alternative explanations of these results. One is that the effect is not due at all to electrostatic changes, but to changes in the local conformation of the inactivation gate. It may be possible to distinguish this hypothesis from the electrostatic one by measuring the effect of more mutant channels with varying degrees of charge in the inactivation gate. The electrostatic hypothesis would be favored over the conformational hypothesis if decreasing charge always speeds inactivation and uncouples it from activation, and increasing charge has the opposite effect. Increasing intracellular ionic strength could undo the effect of charge reduction mutants. Finally, Goldman has recently suggested that the voltage dependence of inactivation might be derived solely from coupling with activation, and that the degree of coupling is determined by the relative rates of inactivation from closed and open states. Thus the changes in inactivation gating we observed in the mutant channels need not imply a physical interaction of the activation and inactivation gates, but might arise simply by changes in the transition rate constants between open, closed and inactivation states [7].

Acknowledgements

For invaluable discussions we thank Drs. D. Cafiso, C.M. Baumgarten, G. Szabo, and E. Perozo, who also aided with the cut-open oocyte voltage clamp. We thank J. Richman for help with the expectation values of exponential functions.

References

[1] P.B. Bennett, K. Yazawa, N. Makita, A.L. George Jr., Nature 376 (1995) 683.
[2] S.C. Cannon, A.I. McClatchey, J.F. Gusella, Pflug. Arch. 423 (1993) 155.
[3] M. Chahine, A.L. George, M. Zhou, S. Ji, W. Sun, R.L. Barchi, R. Horn, Neuron 12 (1994) 281.
[4] L.Q. Chen, V. Santarelli, R. Horn, R.G. Kallen, J. Gen. Physiol. 108 (1996) 549.
[5] D. Colquhoun, B. Sakmann, J. Physiol. 369 (1985) 501.
[6] M.E. Durieux, M.N. Salafranca, K.R. Lynch, J.R. Moorman, Am. J. Physiol. 263 (1992) C896–C900.
[7] L. Goldman, Biophys. J. 76 (1999) 2553.
[8] B. Hille (Ed.), Ionic Channels of Excitable Membranes, Sinauer Associates, Sunderland, MA, 1992.
[9] A.L. Hodgkin, A.F. Huxley, J. Physiol. 117 (1952) 500.
[10] A.L. Hodgkin, A.F. Huxley, J. Physiol. 116 (1952) 497.
[11] T. Hoshi, W.N. Zagotta, R.W. Aldrich, Science 250 (1990) 533.
[12] L.L. Isom, K.S. De Jongh, D.E. Patton, B.F.X. Reber, J. Offord, H. Charbonneau, K. Walsh, A.L. Goldin, W.A. Catterall, Science 256 (1992) 839.
[13] S. Ji, W. Sun, A.L. George Jr., R. Horn, R.L. Barchi, J. Gen. Physiol. 104 (1994) 625.
[14] S. Kellenberger, J.W. West, W.A. Catterall, T. Scheuer, J. Gen. Physiol. 109 (1997) 607.
[15] S. Kellenberger, J.W. West, T. Scheuer, W.A. Catterall, J. Gen. Physiol. 109 (1997) 589.
[16] K.J. Kontis, A. Rounaghi, A.L. Goldin, J. Gen. Physiol. 110 (1997) 391.
[17] T.A. Kunkel, Proc. Natl. Acad. Sci. USA 82 (1985) 488.
[18] D.E. Logothetis, S. Movahedi, C. Satler, K. Lindpaintner, B. Nadal-Ginard, Neuron 8 (1992) 531.
[19] J.R. Moorman, G.E. Kirsch, A.M. Brown, R.H. Joho, Science 250 (1990) 688.
[20] J.R. Moorman, G.E. Kirsch, A.M.J. VanDongen, R.H. Joho, A.M. Brown, Neuron 4 (1990) 243.
[21] J.P. Mounsey, P. Xu, J.E. John, L.T. Horne, J. Gilbert, A.D. Roses, J.R. Moorman, J. Clin. Invest. 95 (1995) 2379.
[22] R.D. Murrell-Lagnado, R.W. Aldrich, J. Gen. Physiol. 102 (1993) 977.
[23] R. Numann, W.A. Catterall, T. Scheuer, Science 254 (1991) 115.
[24] H.B. Nuss, N. Chiamvimonvat, M.T. Perez-Garcia, G.F. Tomaselli, E. Marban, J. Gen. Physiol. 106 (1995) 1171.
[25] H.B. Nuss, N. G Kambouris, E. Marban, G.F. Tomaselli, J.R. Balser, Biophys. J. 78 (2000) 200.
[26] P.C. O'Brien, Biometrics 40 (1984) 1079.
[27] M.E. O'Leary, L.Q. Chen, R.G. Kallen, R. Horn, J. Gen. Physiol. 106 (1995) 641.
[28] D.M. Papazian, L.C. Timpe, Y.N. Jan, L.Y. Jan, Nature 349 (1991) 305.
[29] J. Patlak, Physiol. Rev. 71 (1991) 1047.
[30] D.E. Patton, J.W. West, W.A. Catterall, A.L. Goldin, Proc. Natl. Acad. Sci. USA 89 (1992) 10905.
[31] E. Perozo, D.M. Papazian, E. Stefani, F. Bezanilla, Biophys. J. 62 (1992) 160.
[32] M.R. Smith, A.L. Goldin, Biophys. J. 73 (1997) 1885.
[33] W. Stuhmer, F. Conti, H. Suzuki, X.D. Wang, M. Noda, N. Yahagi, H. Kubo, S. Numa, Nature 339 (1989) 597.
[34] W. Stühmer, F. Conti, H. Suzuki, X. Wang, M. Noda, N. Yahagi, H. Kubo, S. Numa, Nature 339 (1989) 597.
[35] M. Taglialatela, L. Toro, E. Stefani, Biophys. J. 61 (1992) 78.
[36] L. Tang, R.G. Kallen, R. Horn, J. Gen. Physiol. 108 (1996) 89.
[37] A.M.J. VanDongen, Biophys. J. 70 (1996) 1303.
[38] D.W. Wang, A.L.J. George, P.B. Bennett, Biophys. J. 70 (1996) 238.
[39] J.W. West, R. Numann, B.J. Murphy, T. Scheuer, W.A. Catterall, Science 254 (1991) 866.
[40] J.W. West, D.E. Patton, T. Scheuer, Y. Wang, A.L. Goldin, W.A. Catterall, Proc. Natl. Acad. Sci. USA 89 (1992) 10910.
[41] N. Yang, R. Horn, Neuron 15 (1995) 213.
[42] J. Zhou, J.F. Potts, J.S. Trimmer, W.S. Agnew, F.J. Sigworth, Neuron 7 (1991) 775.